scientific reports

Check for updates

OPEN

Sulfasalazine induces ferroptosis in osteosarcomas by regulating Nrf2/SLC7A11/GPX4 signaling axis

Qingqing Qin[1,5], Huaibin Zhang[1,5], Min Lai[1], Jiantong Wei[2], Jun Qian[2], Xingchao Chen[2], Xin Wang[1,3]✉ & Yongping Wang[1,4]✉

Osteosarcoma (OS), a highly malignant primary bone tumor, is characterized by early metastasis, drug resistance, and a resultant poor prognosis, leading to significant disability and mortality. While diverse treatment modalities exist, their therapeutic efficacy remains limited, underscoring the urgent need to investigate effective targeted therapies. Sulfasalazine (SAS), a commonly used anti-inflammatory drug prescribed for nonspecific gastrointestinal diseases, autoimmune rheumatic diseases, ankylosing spondylitis, and various skin conditions, has recently garnered attention for its potential as an anti-tumor agent, specifically its ability to induce ferroptosis, a novel form of regulated cell death. This presents a promising new avenue for OS treatment. Ferroptosis plays a critical role in the malignant progression of OS by regulating iron homeostasis and oxidative stress. To explore the potential of SAS to induce ferroptosis in OS cells, we employed a combined approach of network pharmacological analysis and molecular docking simulations. Network pharmacological analysis identified significant overlap among key target genes of SAS, ferroptosis, and OS, suggesting a multifaceted mechanism of action. Molecular docking simulations further corroborated the hypothesis that SAS targets ferroptosis pathways in OS, solidifying the rationale for further investigation. Our results demonstrate that SAS significantly inhibited the proliferation and migration of OS cells, inducing apoptosis and effectively attenuating their malignant progression. Notably, SAS-treated OS cells displayed hallmarks of ferroptosis, including iron accumulation, elevated levels of malondialdehyde and reactive oxygen species, and reduced levels of glutathione and superoxide dismutase. To confirm the involvement of ferroptosis, we treated SAS-exposed OS cells with the ferroptosis inhibitors DFO, Fer-1, and Lip-1, which reversed the inhibitory effects of SAS on cell activity, further supporting the conclusion that SAS triggers ferroptosis in these cells. We additionally observed that SAS decreased mitochondrial membrane potential in OS cells, potentially indicating mitochondrial damage during ferroptosis. Mechanistically, we found that SAS induced ferroptosis by downregulating the expression of NRF2, subsequently decreasing the expression of the light chain subunit of the cysteine/glutamate transporter system Xc- (SLC7A11) and glutathione peroxidase 4. Collectively, these findings demonstrate that SAS triggers ferroptosis through the NRF2/SLC7A11/GPX4 signaling axis, thereby inhibiting the biological activity of OS cells. This research provides a strong experimental basis for the potential of SAS as a candidate drug for OS treatment and offers a novel targeted therapeutic strategy for this disease.

Keywords Osteosarcoma, Sulfasalazine, Ferroptosis, NRF2, SLC7A11, GPX4

Osteosarcoma (OS) is the most common primary malignant bone tumor and originates from primitive mesenchymal cells. While OS can develop in any bone, it predominantly affects the metaphysis of long bones, particularly the distal femur, proximal tibia, and proximal humerus[1]. The incidence of OS peaks in adolescents around 16 years of age, often presenting with localized pain followed by swelling and restricted joint movement[2]. Although some studies suggest associations between OS and rapid bone growth, radiation exposure from alkylating agents, and certain genetic diseases, the etiology remains unclear in most patients[1,3,4].

[1]The First School of Clinical Medicine, Lanzhou University, Lanzhou 730000, China. [2]Department of Orthopedics, Zhangye People's Hospital affiliated to Hexi College, Zhangye 734000, China. [3]Department of Orthopedics, The First Hospital of Lanzhou University, Lanzhou 730000, China. [4]Department of Orthopedics, the Second Affiliated Hospital of Hainan Medical University, Haikou 570311, China. [5]Qingqing Qin and Huaibin Zhang contributed equally to this work. ✉email: wangxinldyy@126.com; wangyp312@163.com

OS is characterized by a high propensity for local invasion and distant metastasis, with the lungs being the most frequent site. Notably, over 90% of patients who do not receive chemotherapy succumb to pulmonary metastasis[1,5]. Current treatment strategies for OS involve neoadjuvant chemotherapy, surgical resection of both the primary tumor and metastases, and postoperative adjuvant chemotherapy[6,7]. Commonly used chemotherapeutic agents include methotrexate, adriamycin, cisplatin, and ifosfamide[8]. Despite these multimodal approaches, the 5-year overall survival rate for OS has remained relatively constant at 65–70% over the past two decades. The prognosis for patients with metastatic disease is considerably poorer, with a 5-year survival rate of approximately 20%, thereby underscoring the exigent need for innovative therapeutic agents and treatment paradigms to enhance patient outcomes.

Sulfasalazine (SAS), a compound composed of salicylic acid and sulfapyridine, is a commonly prescribed anti-inflammatory drug for the clinical management of nonspecific gastrointestinal disorders, autoimmune rheumatic diseases, ankylosing spondylitis, and certain dermatological conditions[9–11]. Emerging evidence suggests that SAS possesses not only anti-inflammatory properties but also therapeutic potential in diverse cancers. Specifically, SAS can inhibit cysteine import and induce ferroptosis via the system Xc- pathway, thereby suppressing the proliferation and metastasis of gastric and endometrial cancer cells[12,13]. For example, SAS treatment inhibited esophageal cancer TE-1 cell proliferation and significantly reduced xCT and glutathione peroxidase 4(GPX4) mRNA and protein expression; these effects were partially reversed by the addition of ferrostatin-1, a ferroptosis inhibitor[14]. Similarly, SAS significantly reduced oxidative stress resistance in triple-negative breast cancer cells by targeting system Xc- to deplete glutathione (GSH), resulting in ferroptosis[15]. As a key target of SAS, system Xc- can suppress the progression of various malignancies by inhibiting cysteine uptake, depleting intracellular GSH, and promoting reactive oxygen species (ROS) accumulation. These collective findings support the hypothesis that SAS's anticancer activity may be mediated, at least in part, through the induction of ferroptosis.

Ferroptosis, a distinct form of regulated cell death, is mechanistically differentiated from apoptosis, autophagy, and pyroptosis by its dependence on iron and the accumulation of lipid peroxides(LP) at the cell membrane[16]. Morphologically, ferroptotic cells are characterized by cellular swelling, membrane disruption, and mitochondrial shrinkage with cristae reduction, contrasting with the apoptotic features of cell shrinkage, preserved membrane integrity, chromatin condensation, and apoptotic body formation. The core mechanism involves the Fenton reaction, in which iron ions generate excess ROS, driving a LP cascade. In contrast to autophagy and pyroptosis, characterized by autophagosome formation and enhanced lysosomal activity, or membrane rupture with chromatin condensation, respectively[17,18], dysregulation of iron metabolism, ROS overproduction, and aberrant LP activation are recognized hallmarks of ferroptosis. Ferroptosis can be triggered through extrinsic or intrinsic pathways. Extrinsic mechanisms involve inhibition of cell membrane transporters, such as the cystine/glutamate transporter (system Xc^{-}), or activation of iron export proteins, including ferroportin, serum transferrin, and lactotransferrin. Conversely, intrinsic mechanisms involve the blockade of intracellular antioxidant enzymes, such as GPX4[19]. The cystine/glutamate antiporter system Xc^{-}, composed of SLC7A11 (light chain) and SLC3A2 (heavy chain) subunits, is a key regulator of ferroptosis. SLC7A11 promotes GSH synthesis by mediating cystine influx, thereby enhancing GPX4's inhibitory effect on ferroptosis[20]. This process plays a significant role in the progression of gastric, hepatic, and breast cancers[21–23], and inducing ferroptosis in tumor cells can inhibit their advancement. Furthermore, ferroptosis is a key regulatory node in the pathogenesis, progression, and treatment of OS[24–26]. NRF2, an upstream regulator of SLC7A11, promotes tumor cell survival by upregulating SLC7A11 expression, thereby exacerbating malignancy. Consequently, inhibiting the NRF2 signaling pathway to downregulate the SLC7A11/GPX4 axis represents a potential therapeutic strategy to induce ferroptosis and inhibit OS progression.

This study demonstrated that SAS inhibits OS cell progression by inducing ferroptosis. We further identified the NRF2/SLC7A11/GPX4 signaling pathway as a key mediator of SAS's effects on OS. These findings elucidate a novel mechanism underlying the anti-OS activity of SAS, supporting its potential as a therapeutic agent for OS treatment.

Materials and methods

SAS, ferroptosis, and target identification in OS

The molecular structure of SAS was obtained from the PubChem database (https://pubchem.ncbi.nlm.nih.gov/). Potential SAS targets were predicted using the PharmMapper (https://www.lilab-ecust.cn/pharmmapper/)SwissTargetPrediction (https://www.swisstargetprediction.ch/), and SEA (https://sea.bkslab.org/) databases. Ferroptosis-related gene targets were retrieved from the GeneCards database (https://www.genecards.org/). OS-associated targets were identified in the GeneCards, DisGeNET (https://www.disgenet.org/), and OMIM databases (https://www.omim.org/), using "osteosarcoma" as the search term. Overlapping targets among OS, ferroptosis, and SAS were identified using Venny 2.1 (https://bioinfogp.cnb.csic.es/tools/venny/), representing potential mechanisms by which SAS may modulate ferroptosis in the treatment of OS.

Protein–protein interaction network construction and GO/KEGG enrichment analysis

Common target genes were input into the STRING database (https://string-db.org/), with the species limited to Homo sapiens. The resulting data were imported into Cytoscape 3.10.3 to construct a protein–protein interaction (PPI) network. To identify and visualize key genes, the Centiscape 2.2 plugin was utilized to calculate gene degree, proximity centrality, and betweenness centrality based on these metrics. Gene Ontology (GO) and Kyoto Encyclopedia of Genes and Genomes (KEGG) enrichment analyses of the common target genes were performed using the DAVID database (https://david.ncifcrf.gov/). GO analysis encompassed biological process (BP), cellular component (CC), and molecular function (MF) categories.

Molecular docking

The structure of SAS in SDF format was retrieved from the PubChem database. Accession numbers of target proteins were obtained from the UniProt database (https://www.uniprot.org/), and the corresponding three-dimensional structures were acquired from the Protein Data Bank (PDB; https://www.rcsb.org/). Target protein structures were prepared using PyMOL software by removing water molecules and any bound ligands. Using AutoDock Tools 1.5.7, hydrogen atoms were added, and partial charges were assigned; the prepared structures were then saved in pdbqt format. Molecular docking was performed using AutoDock Vina 2.0, and binding energies were calculated. The resulting interactions were visualized using PyMOL software.

Reagents and antibodies

SAS was obtained from Sigma-Aldrich (St. Louis, Missouri, USA). Deferoxamine (DFO), liproxstatin-1 (Lip-1), and ferrostatin-1 (Fer-1) were purchased from MCE (New Jersey, USA). A panel of primary antibodies was used for the experiments. These included GAPDH (1:1000; Boster, Wuhan, China), ferritin heavy chain 1 (FTH1) (1:1000; Proteintech, Wuhan, China), nuclear factor erythroid 2-related factor 2 (NRF2) (1:1000; Boster, Wuhan, China), solute carrier family 7 member 11 (SLC7A11) (1:1000; Proteintech, Wuhan, China), and GPX4 (1:1000; Proteintech, Wuhan, China).

Cell culture

The human OS cell lines MG63 and U2OS were used in this study. MG63 cells, obtained from Servicebio (Wuhan, China), were cultured in Dulbecco's Modified Eagle Medium (DMEM) supplemented with non-essential amino acids (NEAA). U2OS cells, obtained from Pricella (Wuhan, China), were cultured in McCoy's 5A medium. Both culture media were supplemented with 10% fetal bovine serum and 1% penicillin–streptomycin (1000 μg/mL streptomycin + 100 U/mL penicillin). The cells were maintained in a humidified incubator at 37 °C with 5% CO_2. The medium was replaced regularly based on visual observation of the medium color.

Cell viability

Cell viability was assessed using the Cell Counting Kit-8 (CCK-8; BioScience, Shanghai, China). Absorbance at 450 nm was measured using a microplate reader (Thermo Fisher, China), and cell viability was calculated as follows:

$$Cell\ viability(\%) = \left[\left(A_{sample} - A_{blank}\right) / \left(A_{control} - A_{blank}\right)\right] \times 100$$

Cell proliferation assay

MG63 and U2OS cells were seeded in 96-well plates at a density of 5000 cells per well and allowed to attach. Following attachment, the cells were treated with a range of SAS concentrations for 24 h. Cell proliferation was assessed using an EdU kit (Abbkine, Wuhan, China). Specifically, after treatment with the EdU cell proliferation assay reagent according to the manufacturer's instructions, images were captured using a fluorescence microscope (Olympus, Germany) and analyzed.

Flow cytometry examination

For cell cycle analysis, MG63 and U2OS cells(1×10^6 per well) were seeded per well in 6-well plates and treated with 0.25, 0.5, and 1.0 mM SAS for 24 h. The cells were then harvested and analyzed by flow cytometry (BD Biosciences, USA) using a cell cycle staining kit (Multi Sciences, Shanghai, China). Apoptosis was also assessed by flow cytometry using an Annexin V-FITC apoptosis detection kit (Multi Sciences, Shanghai, China). In addition, mitochondrial membrane potential (MMP) was measured using a JC-1 fluorescent probe (Beyotime, Shanghai, China) and analyzed by flow cytometry. Finally, ROS levels were determined using an ROS detection kit (Jian Cheng, Nanjing, China) and analyzed by flow cytometry.

Cell migration assay

Cell migration was assessed using both scratch and Transwell assays. In vitro scratch assays were performed as follows: MG63 and U2OS cells were seeded in six-well plates and grown to confluence. A scratch was then created using a 200 μL pipette tip, and the cells were treated with various concentrations of SAS. Cell migration into the scratched area was observed and photographed using an inverted microscope (Nikon, Shanghai, China) at 0 and 24 h. For Transwell assays, 200 μL of cell suspension was added to the upper chamber and 600 μL of complete medium containing 20% FBS was added to the lower chamber. Following incubation, cells that had migrated to the lower surface of the membrane were fixed, stained, observed, and photographed using an inverted microscope.

Ferrous iron assay

MG63 and U2OS cells were evenly seeded in six-well plates and allowed to attach. Following attachment, the cells were treated with a range of SAS concentrations and incubated for 24 h. After incubation, ferrous iron levels were quantified using a ferrous ion assay kit (Solarbio, Beijing, China), and absorbance values were measured at 510 nm using a microplate reader.

GSH assay

MG63 and U2OS cells were evenly seeded in six-well plates and allowed to attach. Following attachment, the cells were treated with 0.0 mM, 0.25 mM, 0.5 mM, and 1.0 mM SAS and incubated for 24 h. After incubation, the cells were divided into two groups. One group was used for protein concentration determination, as described below. The remaining cells were disrupted by manual homogenization, and GSH levels were quantified using a

GSH assay kit (Jian Cheng, Nanjing, China). Absorbance values were measured at 405 nm using a microplate reader.

SOD assay

MG63 and U2OS cells were evenly seeded in six-well plates and allowed to attach. Following attachment, the cells were treated with a range of SAS concentrations and incubated for 24 h. After incubation, the cells were harvested, and an appropriate volume of PBS buffer was added to the cell pellet. The cells were disrupted by manual homogenization using a glass homogenizer in an ice bath for 3–5 min. Superoxide dismutase (SOD) activity was then quantified using a SOD assay kit (Jian Cheng, Nanjing, China). The kit reagents were then added to a 96-well plate, and the mixture was incubated for 20 min at room temperature. The absorbance values were measured at 450 nm using a microplate reader.

MDA assay

MG63 and U2OS cells were evenly seeded in six-well plates and allowed to attach. Following attachment, the cells were treated with 0.25 mM, 0.5 mM, and 1.0 mM SAS for 24 h. After incubation, the cells were divided into two groups: one for protein quantification and the other for malondialdehyde(MDA) analysis. For the MDA assay, cells were homogenized, and the MDA assay kit (Jian Cheng, Nanjing, China) reagents were added. Following vortex mixing, the samples were heated at 95 °C for 40 min, cooled in running water, and centrifuged at 4000 × *g* for 10 min. The supernatant (0.25 mL) was then transferred to a 96-well plate, and absorbance was measured at 530 nm using a microplate reader.

Western blot analysis

MG63 and U2OS cells were treated with various concentrations of SAS for 24 h, harvested, and lysed using RIPA lysis buffer (Epizyme, Shanghai, China) supplemented with a protease inhibitor. Protein concentration was determined using a BCA protein assay kit (Epizyme, Shanghai, China). Equal amounts of protein were separated by SDS-PAGE, transferred to PVDF membranes, and blocked with 5% skim milk (Epizyme, Shanghai, China) for 1.5 h. The membranes were incubated with primary antibody at 4 °C overnight, washed three times with TBST (Servicebio, Wuhan, China), and incubated with secondary antibody for 1 h at room temperature. Protein bands were visualized using a chemiluminescence detection kit (Epizyme, Shanghai, China).

Real-time quantitative PCR (RT-qPCR)

Total RNA was extracted from cells using TRIzol reagent (Takara, Japan) and reverse transcribed into cDNA. RT-qPCR was performed using a thermal cycling protocol. This protocol consisted of an initial denaturation step at 95 °C for 35 s, followed by 40 cycles of denaturation at 95 °C for 5 s and annealing at 60 °C for 34 s. Relative gene expression was calculated using the $2^{-\Delta\Delta Ct}$ method (target genes listed in Table 1).

Statistical analysis

Experimental data were analyzed using SPSS version 26.0 and GraphPad Prism version 8. Data are presented as mean ± standard deviation (SD). Statistical significance was determined by one-way ANOVA or Student's t-test, as appropriate. A P value of < 0.05 was considered statistically significant.

Results

Network pharmacological analysis of SAS, ferroptosis, and OS

Potential targets of SAS were predicted using the PharmMapper, SwissTargetPrediction, and SEA databases, yielding 290, 100, and 89 targets, respectively. After removing duplicate entries, a total of 424 potential SAS targets were identified. Gene targets related to ferroptosis were retrieved from the GeneCards database, resulting in 1516 targets. OS-related targets were obtained from the GeneCards, DisGeNET, and OMIM databases. Applying a Score > 1.0 as the selection criterion, 1163 potential targets were identified in GeneCards. DisGeNET and OMIM yielded 1024 and 11 disease-related targets, respectively. After removing duplicate entries across these three databases, a total of 1596 OS-related targets were identified. Intersecting the target genes of SAS, ferroptosis, and OS resulted in 35 common target genes, visualized using a Venn diagram generated with Venny (Fig. 1A). Analysis of the PPI network of these 35 targets using Cytoscape 3.10.3 revealed a network comprising 35 nodes and 243 edges (Fig. 1B). Employing thresholds of Degree unDir > 13.88571429, Betweenness

Gene	Primer sequence
GAPDH-F	5'-CATCTTCTTGTGCAGTGCC-3'
GAPDH-R	5'-ACCAGCTTCCCATTCTCAG-3'
NRF2-F	5'-GTATGCAACAGGACATTGAGCAAG-3'
NRF2-R	5'-TGGAACCATGGTAGTCTCAACCAG-3'
SLC7A11-F	5'-GCAGTTGCTGGGCTGATTT-3'
SLC7A11-R	5'-CTGTACTAAATGGGTCCGAATAGAG-3'
GPX4-F	5'-TGGCCTTCCCGTGTAACCAG-3'
GPX4-R	5'-CCGTTCACGCAGATCTTGCT-3'

Table1. primer sequence.

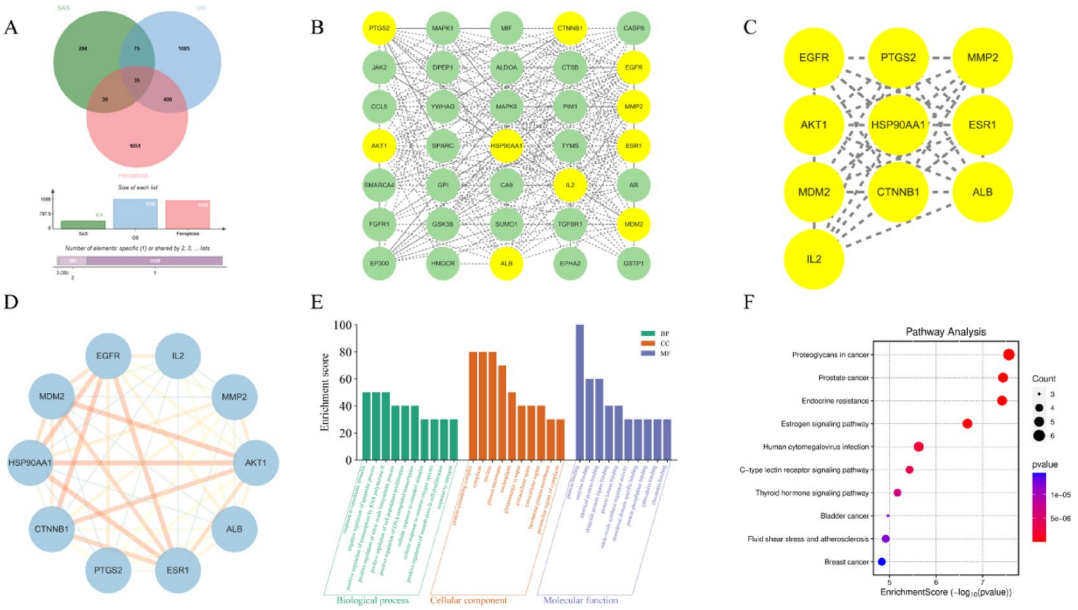

Fig. 1. Network pharmacological analysis of SAS, ferroptosis, and OS. (**A**) Venn diagram illustrating common target genes among SAS, ferroptosis, and OS. (**B**) PPI network of OS targets modulated by SAS via ferroptosis. (**C**) Core target genes involved in SAS-mediated ferroptosis in OS. (**D**) PPI network highlighting core target genes through which SAS modulates ferroptosis in OS. (**E**) GO enrichment analysis results. (**F**) KEGG pathway enrichment analysis results.

unDir > 21.82857143, and Closeness unDir > 0.018523047, ten key genes were identified (Fig. 1C), forming a sub-network of 10 nodes and 45 edges (Fig. 1D). Line thickness, color intensity, and combined score in the network diagram are proportional to the combined score value. Key target genes included MDM2, EGFR, PTGS2, and AKT1 (Fig. 1D). GO enrichment analysis was performed on the identified intersection targets related to SAS treatment of OS via ferroptosis using the David database. As illustrated in Fig. 1E, GO enrichment analysis revealed that BP primarily encompassed response to xenobiotic stimulus, negative regulation of apoptotic process, positive regulation of transcription by RNA polymerase II, positive regulation of nitric oxide biosynthetic process, positive regulation of cell population proliferation, positive regulation of DNA-templated transcription, cellular response to estradiol stimulus, cellular response to reactive oxygen species, positive regulation of smooth muscle cell proliferation, and response to estrogen. CC analysis indicated enrichment in protein-containing complex, cytoplasm, nucleus, plasma membrane, nucleoplasm, glutamatergic synapse, extracellular space, extracellular region, basolateral plasma membrane, and perinuclear region of cytoplasm. MF analysis highlighted protein binding, enzyme binding, identical protein binding, ubiquitin protein ligase binding, protein kinase binding, nitric oxide synthase regulator activity, disordered domain specific binding, protein phosphatase binding, calmodulin binding, and chromatin binding. KEGG pathway enrichment analysis revealed a significant enrichment in pathways including proteoglycans in cancer, prostate cancer, endocrine resistance, estrogen signaling pathway, human cytomegalovirus infection, C-type lectin receptor signaling pathway, thyroid hormone signaling pathway, bladder cancer, fluid shear stress and atherosclerosis, and breast cancer (Fig. 1F)[27–29].

Molecular docking of SAS with ferroptosis and OS target genes

To evaluate the potential binding affinity of SAS to key target proteins—including MDM2, EGFR, PTGS2, and AKT1—molecular docking simulations were performed. The resulting interactions were visualized using PyMOL software (Fig. 2). Binding energy values were used to assess the binding strength between SAS and each target protein, where lower binding energy indicates a stronger, more favorable interaction. The binding energies of SAS with MDM2, EGFR, PTGS2, and AKT1 were −7.7, −3.1, −9.4, and −6.7 kcal/mol, respectively, indicating that SAS exhibits the strongest binding affinity for PTGS2.

SAS inhibits OS cell viability

To evaluate the effects of SAS on OS cell viability, MG63 and U2OS cells were treated with SAS (0, 0.25, 0.5, 0.75, 1.0, 1.5, and 2.0 mM) for 24, 48, and 72 h. The chemical structure of SAS is shown in Fig. 3A. Cell viability was measured using the CCK-8 assay (Fig. 3B). As demonstrated in Fig. 3C and D, SAS inhibited OS cell viability in a concentration- and time-dependent manner. The half-maximal inhibitory concentrations (IC50) of SAS against MG63 cells were 0.58 mM, 0.38 mM, and 0.22 mM at 24, 48, and 72 h, respectively. Comparable values for U2OS cells were 0.61 mM, 0.33 mM, and 0.24 mM at the same time points. Subsequent analyses utilized SAS at 0.25, 0.5, and 1.0 mM, with both cell lines exposed for 24 h.

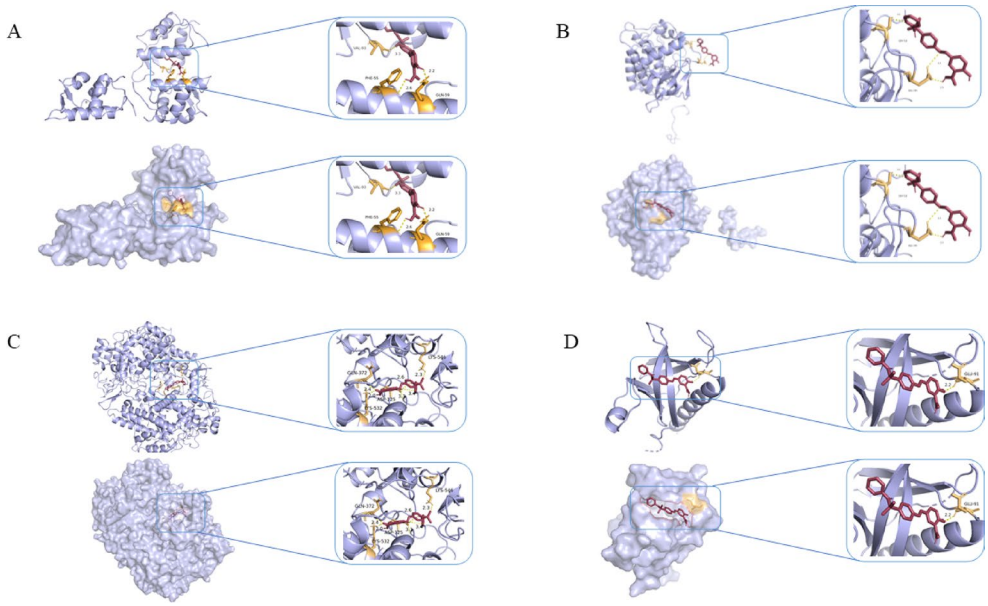

Fig. 2. Molecular docking of sulfasalazine (SAS) with osteosarcoma target gene molecules. Docking poses of SAS with (**A**) MDM2, (**B**) EGFR, (**C**) PTGS2, and (**D**) AKT1.

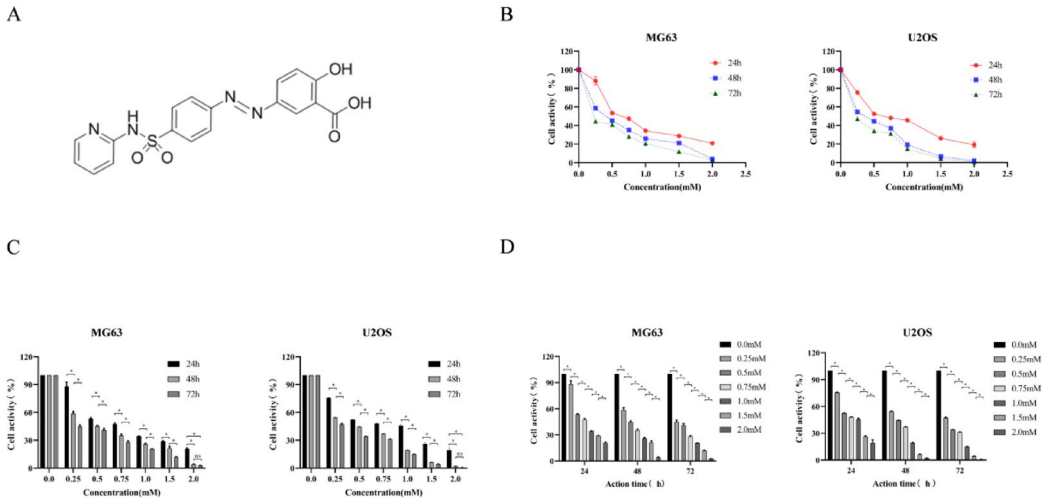

Fig. 3. SAS inhibits OS cell viability. (**A**) Chemical structure of SAS. (**B**) Viability of MG63 and U2OS cells treated with SAS for 24, 48, and 72 h, as determined by CCK-8 assay. (**C**, **D**) Statistical analysis comparing the effects of varying SAS treatment durations at a fixed concentration (**C**) and varying SAS concentrations at a fixed duration (**D**) on the viability of MG63 and U2OS cells. (Data were presented as mean ± SD, n = 3; $^{*}P < 0.05$. ns, no statistical significance.)

Effect of SAS on OS cell behavior

To investigate the effects of SAS on OS cell behavior, MG63 and U2OS cells were treated with 0.25, 0.5, and 1.0 mM SAS for 24 h. Our results indicated that SAS significantly inhibited cell proliferation, as demonstrated by EDU assays (Fig. 4A) .Further analysis of cell cycle distribution (Fig. 4B) revealed G1 phase arrest following SAS treatment. Furthermore, wound-healing assays (Fig. 4C) and Transwell assays (Fig. 4D) indicated that SAS inhibited cell migration in a concentration-dependent manner. Finally, flow cytometric analysis (Fig. 4E) showed that SAS induced apoptosis in a concentration-dependent manner. These findings collectively demonstrate that SAS suppressed multiple aspects of OS cell malignant behavior.

SAS induced cell death via triggering ferroptosis

We next investigated whether SAS induces ferroptosis in OS cells. MG63 and U2OS cells were treated with 0.5 mM SAS for 24 h, with or without the ferroptosis inhibitors DFO, Fer-1, and Lip-1. As shown in Fig. 5A, SAS significantly reduced cell viability, an effect that was partially reversed by co-treatment with these inhibitors.

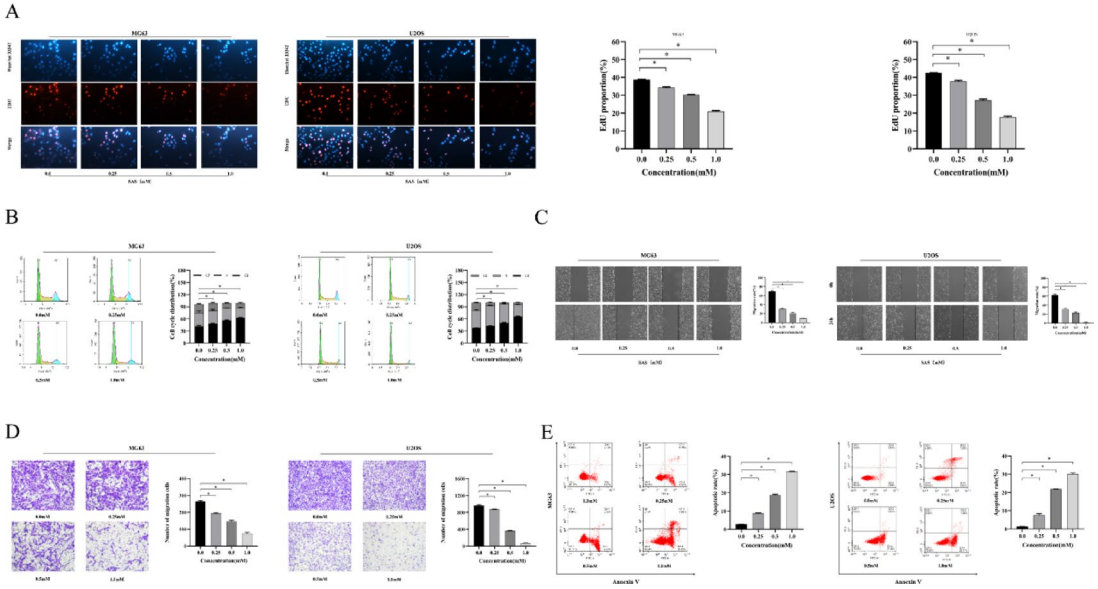

Fig. 4. Effect of SAS on OS Cell Behavior. (**A**) EDU staining assay showing the effect of 24-h SAS treatment on MG63 and U2OS cell proliferation. (**B**) Cell cycle distribution in MG63 and U2OS cells following 24-h SAS treatment, as determined by flow cytometry. Statistical analysis was performed to quantify the proportion of cells in the G1 phase across all experimental groups. (**C**) Representative images of MG63 and U2OS cells treated with various concentrations of SAS for 24 h, illustrating the effect on cell migration. (**D**) Quantification of cell migration in MG63 and U2OS cells following 24-h treatment with various concentrations of SAS. (**E**) Apoptosis rate in MG63 and U2OS cells following 24-h SAS treatment, as determined by flow cytometry. (Data were presented as mean ± SD, n = 3. $^{*}P < 0.05$ versus control group.)

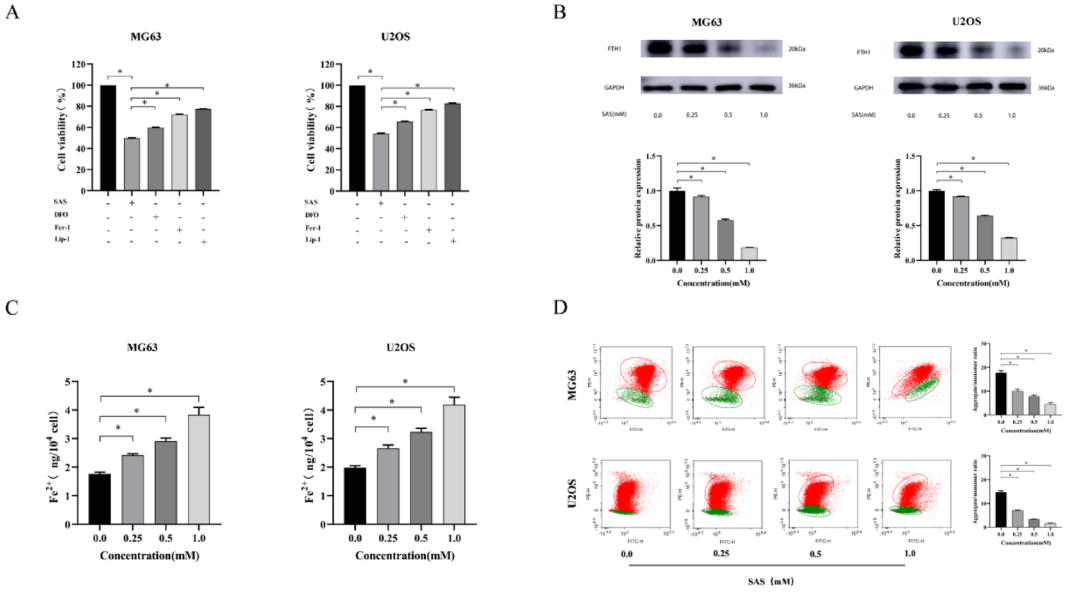

Fig. 5. SAS induced cell death via triggering ferroptosis. (**A**) Effect of 24-h treatment with ferroptosis inhibitors (DFO, Fer-1, Lip-1) on the viability of MG63 and U2OS cells, as determined by CCK-8 assay. (**B**) Western blot analysis of FTH1 protein expression in MG63 and U2OS cells following 24-h SAS treatment. (**C**) Intracellular Fe2 + levels in MG63 and U2OS cells following 24-h SAS treatment. (**D**) Mitochondrial membrane potential (MMP) in MG63 and U2OS cells following 24-h SAS treatment, as determined by flow cytometry. (Data were presented as mean ± SD, n = 3; $^{*}P < 0.05$.)

Furthermore, SAS treatment decreased FTH1 protein expression and increased Fe^{2+} release in a concentration-dependent manner (Fig. 5B and C). Consistent with ferroptosis induction, SAS also decreased MMP in a concentration-dependent manner (Fig. 5D). Taken together, these findings strongly suggest that SAS induces ferroptosis in OS cells.

SAS induces ferroptosis in OS cells

To further investigate the role of ferroptosis in the anti-cancer activity of SAS, we evaluated key ferroptosis markers in MG63 and U2OS cells treated with 0, 0.25, 0.5, and 1.0 mM SAS for 24 h. Consistent with ferroptosis induction, GSH levels decreased in a concentration-dependent manner (Fig. 6A). Similarly, superoxide SOD expression was reduced (Fig. 6B). In contrast, MDA levels increased significantly (Fig. 6C), with the most pronounced effect observed at 1.0 mM SAS. Furthermore, ROS levels also increased in a concentration-dependent manner (Fig. 6D). These combined findings—specifically, the reduction in the antioxidant enzymes GSH and SOD, along with the increase in LP markers MDA and ROS—support the conclusion that SAS induces ferroptosis in OS cells.

Molecular mechanisms of SAS-induced effects on OS cells

To investigate the molecular mechanisms by which SAS affects OS cells, we assessed the protein expression of NRF2, SLC7A11, and GPX4 in MG63 and U2OS cells treated with 0.25, 0.5, and 1.0 mM SAS for 24 h. SAS treatment resulted in a concentration-dependent decrease in the protein expression of NRF2, SLC7A11, and GPX4 (Fig. 7A). This effect was partially reversed by co-treatment with the NRF2 agonist RTA-408, which increased the expression of these proteins (Fig. 7B). Consistent with these protein findings, SAS also suppressed the mRNA expression of NRF2, SLC7A11, and GPX4 in a concentration-dependent manner (Fig. 7C). Collectively, these findings indicate that SAS exerts its anti-tumor effects in OS cells, at least in part, by modulating the NRF2/SLC7A11/GPX4 signaling pathway.

Discussion

OS is the most common primary malignant bone tumor, characterized by a high propensity for local invasion and metastasis. Current treatment modalities often yield unsatisfactory outcomes, underscoring the need for targeted therapeutic strategies predicated on novel mechanisms of action. Consequently, the development of such strategies has emerged as a key research priority to improve the prognosis of patients with OS. SAS, an FDA-approved anti-inflammatory agent used to treat conditions like Crohn's disease, rheumatoid arthritis, and inflammatory bowel disease, has attracted interest in cancer therapy due to its ability to inhibit system Xc-, deplete cellular GSH, and induce ROS accumulation[2,30]. Notably, analysis of a "drug-ferroptosis-disease" interaction network based on multi-omics data reveals significant gene overlap in key targets of SAS, ferroptosis, and OS. Building on this, topological analysis of the PPI network identified a core target group within the SAS-ferroptosis-OS regulatory network, and GO and KEGG analyses revealed their primary functions. These core targets are predominantly involved in biological processes such as response to xenobiotic stimulus, protein-containing complex assembly, and protein binding, as well as molecular functions including oxidative stress

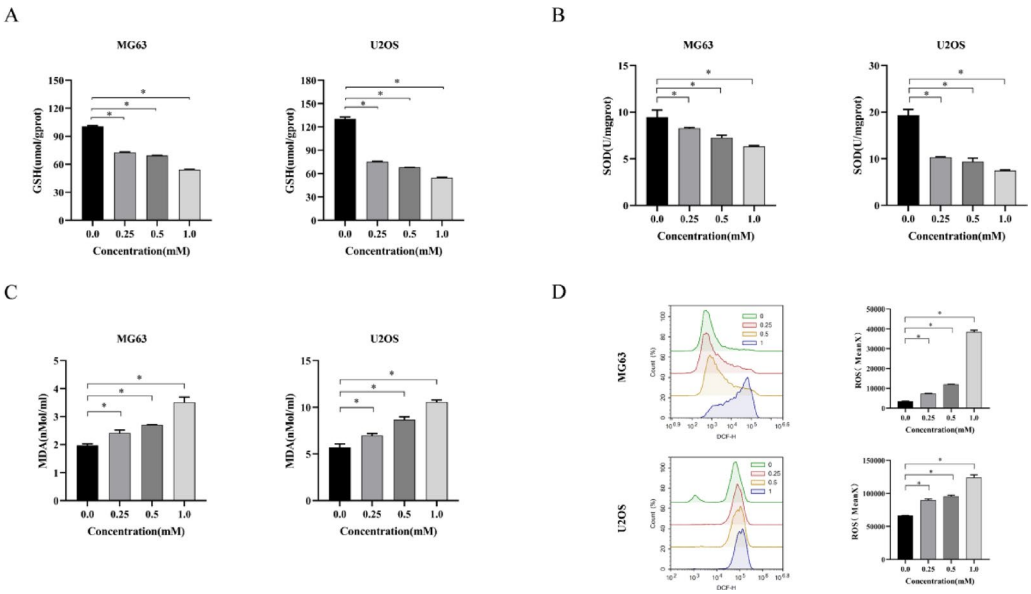

Fig. 6. SAS induces ferroptosis in OS Cells. (**A**) Glutathione (GSH) levels in MG63 and U2OS cells following 24-h SAS treatment. (**B**) Superoxide dismutase (SOD) levels in MG63 and U2OS cells following 24-h SAS treatment. (**C**) Malondialdehyde (MDA) levels in MG63 and U2OS cells following 24-h SAS treatment. (**D**) Reactive oxygen species (ROS) levels in MG63 and U2OS cells following 24-h SAS treatment, as determined by flow cytometry. (Data were presented as mean ± SD, n = 3. $^*P < 0.05$ versus control group.)

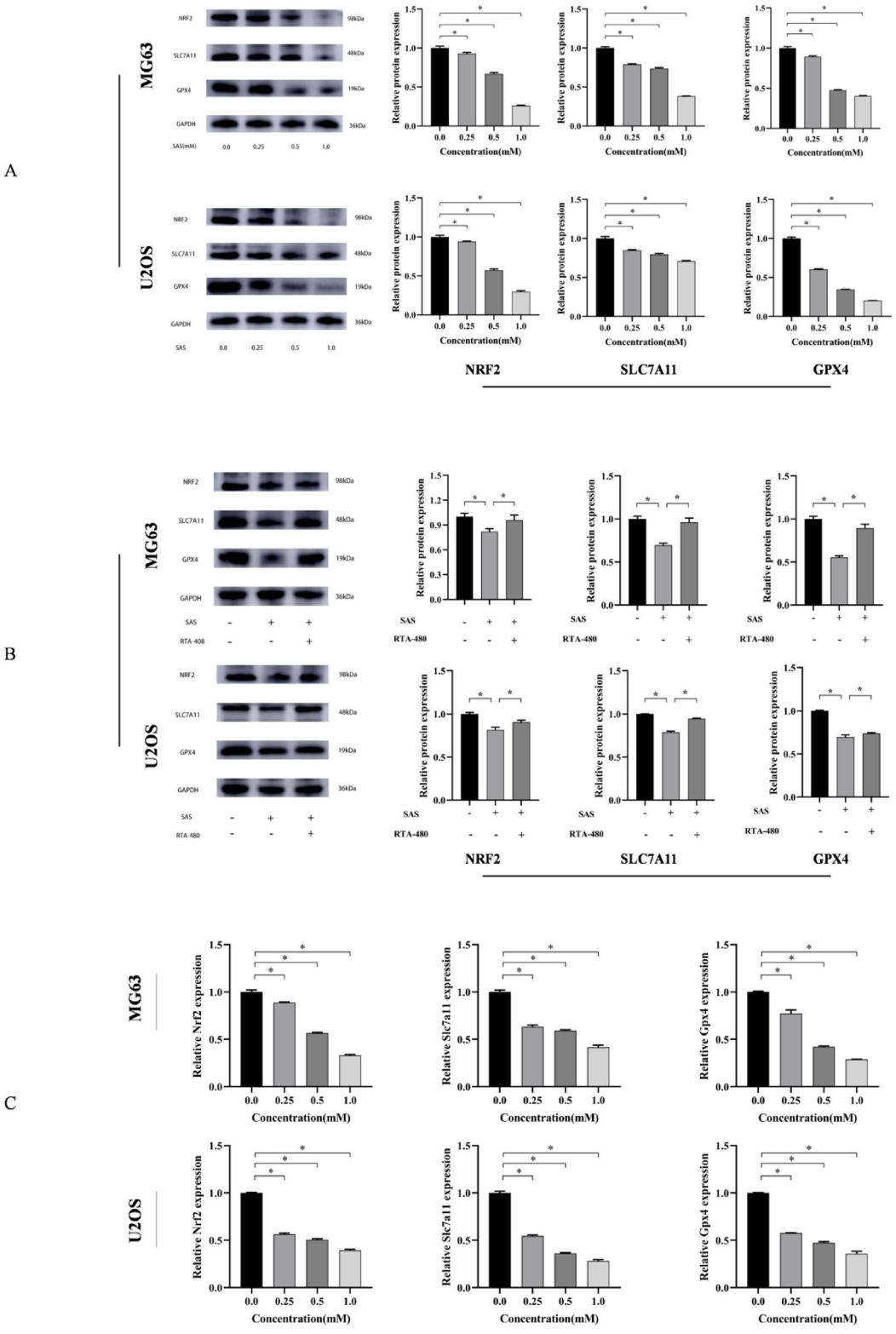

Fig. 7. Molecular Mechanisms of SAS-Induced Effects on OS Cells**.** (**A**) Western blot analysis of NRF2, SLC7A11, and GPX4 protein expression in MG63 and U2OS cells following 24-h SAS treatment. (**B**) Western blot analysis of NRF2, SLC7A11, and GPX4 protein expression in MG63 and U2OS cells following treatment with RTA-480. (**C**) Quantitative PCR (qPCR) analysis of NRF2, SLC7A11, and GPX4 mRNA expression in MG63 and U2OS cells following 24-h SAS treatment. (Data were presented as mean ± SD, n = 3**;** $^{*}P < 0.05$.)

response and cell death regulation. These findings suggest that SAS's effects on these biological processes contribute to its ability to induce ferroptosis in OS cells. These signaling pathways play a pivotal role in the SAS-mediated ferroptotic effect in tumors. In support of these findings, molecular docking simulations of SAS with the protein structures of key target genes, including MDM2, EGFR, PTGS2, and AKT1, further support the potential of SAS to counteract OS via ferroptosis. Given its established clinical safety profile, SAS possesses significant translational potential for drug repurposing in OS-targeted therapy, warranting further efficacy validation through prospective clinical trials. To further investigate the potential of SAS as an OS therapeutic, we conducted in vitro studies to assess its effects on proliferation, migration, and apoptosis of OS cells.

Consistent with these network analyses and molecular docking simulations, this study demonstrated that SAS inhibited OS cell proliferation, inducing G1 cell cycle arrest in MG63 and U2OS cells. Furthermore, SAS suppressed OS cell migration, a critical process in tumor invasion and metastasis. Tumor cell migration facilitates invasion of surrounding tissues and subsequent hematogenous dissemination to distant sites[26], highlighting its importance as a therapeutic target. Consistently, we observed that SAS reduced OS cell migration in a concentration-dependent manner. In addition to inhibiting proliferation and migration, SAS also induced apoptosis in OS cells, further contributing to its anti-tumor effects. Apoptosis, a programmed cell death process crucial for maintaining homeostasis, is often dysregulated in cancer[31–33]. Therefore, its induction represents another avenue for cancer therapy.

To investigate whether ferroptosis plays a role in SAS's anti-OS activity, we treated cells with SAS in combination with known ferroptosis inhibitors. Consistent with SAS inducing ferroptosis, we observed that in OS cells treated with SAS, viability decreased; however, co-treatment with DFO, an iron chelator, along with Fer-1 and Lip-1, which are additional specific ferroptosis inhibitors, partially restored cell viability. Ferroptosis is a distinct form of RCD driven by intracellular iron accumulation. Consequently, inhibiting iron accumulation can prevent ferroptosis. This protective effect, coupled with the concentration-dependent decrease in MMP induced by SAS (compared to control), strongly suggests that SAS exerts its anti-OS activity, at least in part, via ferroptosis induction.

Since ferroptosis is driven by iron accumulation, we next investigated the effects of SAS on key regulators of iron homeostasis, including FTH1. FTH1 is the primary intracellular iron storage protein, forming a complex with ferritin light chain to efficiently bind and store free iron. Iron release from FTH1 is crucial for maintaining cellular iron homeostasis. Normally, cellular iron homeostasis is tightly regulated through processes involving intestinal absorption, red blood cell degradation, and recycling[34,35]. Free Fe^{2+} is oxidized to Fe3 + by ceruloplasmin, binds to transferrin, and undergoes endocytosis. Ultimately, it is reduced back to Fe^{2+} by STEAP3 for storage in labile iron pools and ferritin. However, disruption of this tightly controlled balance can trigger ferroptosis. Consistent with SAS disrupting this homeostasis and inducing ferroptosis, we observed that FTH1 protein expression in OS cells decreased in a concentration-dependent manner following SAS treatment. These findings suggest that SAS disrupts iron homeostasis, leading to the accumulation of Fe^{2+}. In addition to disrupting iron homeostasis, ferroptosis is also characterized by increased oxidative stress and lipid peroxidation. Therefore, we next investigated the effects of SAS on key regulators of oxidative stress, including GSH and SOD, as well as markers of lipid peroxidation and ROS production.

In contrast to the role of oxidative stress in ferroptosis, GSH, a thiol tripeptide composed of glutamate, cysteine, and glycine, functions as a critical antioxidant. Similarly, SOD, another antioxidant enzyme, catalyzes the dismutation of superoxide radicals, mitigating LP. Given that accumulation of LP products and ROS is a hallmark of ferroptosis, we investigated the effect of SAS on these parameters in OS cells. Our results show that SAS treatment reduced GSH and SOD levels, while simultaneously inducing a concentration-dependent increase in both LP and ROS levels. MDA, a major product of LP, served as a marker of ferroptosis in this context. Since GSH synthesis is crucial for mitigating lipid peroxidation, we next investigated the effects of SAS on System xc-, a key regulator of GSH synthesis.

System xc – is a cystine/glutamate antiporter responsible for the equimolar exchange of extracellular cystine for intracellular glutamate. This heterodimeric transporter is composed of two subunits: a heavy chain, solute carrier family 3 member 2 (SLC3A2), and a light chain, solute carrier family 7 member 11 (SLC7A11/xCT). SLC7A11, a multipass transmembrane protein, mediates the antiport activity, while SLC3A2, a single-pass transmembrane protein, stabilizes SLC7A11 and ensures its proper localization within the cell membrane. The activity of System xCT is critically linked to ferroptosis, an iron-dependent form of regulated cell death triggered by the accumulation of LP. Specifically, System xc- promotes the import of cystine, a crucial precursor for the synthesis of GSH. GPX4, a key suppressor of ferroptosis, utilizes GSH to detoxify LP, thereby preventing ferroptosis[36]. Consequently, inhibition or depletion of SLC7A11, which impairs cystine uptake and thus GSH synthesis, has been shown to induce ferroptosis in various cancer cells[37,38]. Conversely, SLC7A11 overexpression enhances GSH synthesis and promotes resistance to ferroptosis. Taken together, these findings underscore the critical role of SLC7A11-mediated cystine uptake in maintaining cellular GSH levels, protecting against ferroptosis, and supporting cellular survival under oxidative stress.

The NRF2/SLC7A11/GPX4 axis plays a crucial role in regulating ferroptosis. NRF2 is a transcription factor that upregulates SLC7A11 expression, which in turn regulates GPX4 activity through its role in GSH synthesis. Consequently, inhibition of this axis promotes ferroptosis and suppresses tumor growth in various cancers[39–42], while activation can inhibit ferroptosis in other disease contexts by increasing GSH synthesis and antioxidant defenses[43–45]. In this study, SAS treatment reduced the protein expression of NRF2, SLC7A11, and GPX4 in MG63 and U2OS cells in a concentration-dependent manner, an effect that was reversed by co-treatment with an NRF2 agonist. Consistent with these protein expression findings, SAS also suppressed the mRNA expression of NRF2, SLC7A11, and GPX4 in a concentration-dependent manner.

These findings suggest that SAS induces ferroptosis in OS cells by disrupting iron homeostasis, increasing oxidative stress, and inhibiting the NRF2/SLC7A11/GPX4 axis, demonstrating promising in vitro anti-OS activity

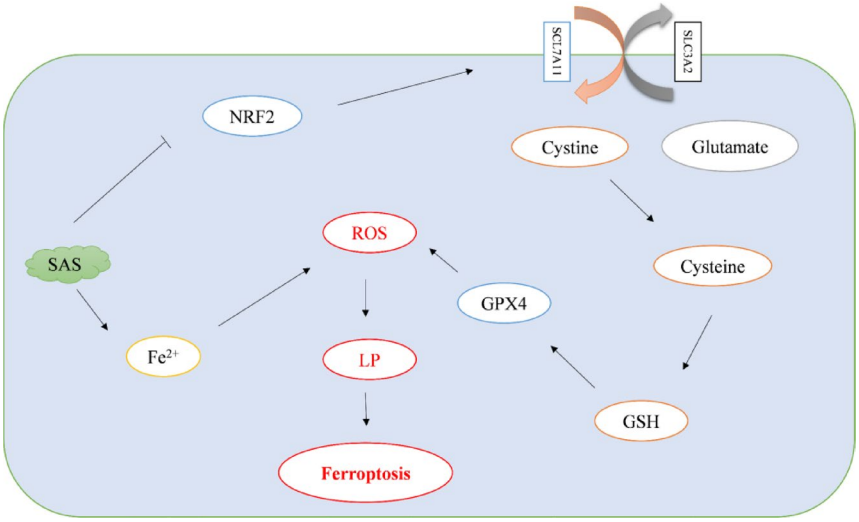

Fig. 8. Schematic diagram displays potential mechanism of SAS-induced ferroptosis in OS cells.

(Fig. 8). Clinical translation faces challenges, despite SAS's favorable safety profile, multitargeted effects, and cost-effectiveness, because effective in vitro concentrations exceed achievable systemic levels. Future strategies should focus on reducing the effective dose via combination therapies with chemotherapeutics or ferroptosis-sensitizing agents (e.g., Erastin or NRF2 inhibitors) and on developing nanocarriers or local sustained-release systems for enhanced drug delivery. This research is limited by the absence of in vivo data and examination of the interplay between SAS-induced ferroptosis and other programmed cell death pathways (e.g., apoptosis, autophagy, and pyroptosis) in OS cells. Future investigations will further elucidate SAS's role and mechanisms in OS.

Data availability

The datasets used and/or analysed during the current study available from the corresponding author on reasonable request.

Received: 28 November 2024; Accepted: 23 July 2025
Published online: 18 August 2025

References

1. Ritter, J. & Bielack, S. S. Osteosarcoma. *Ann Oncol: Off J Eur Soc Med Oncol* **21**(Suppl 7), 320–325 (2010).
2. Chen, C. et al. Immunotherapy for osteosarcoma: Fundamental mechanism, rationale, and recent breakthroughs. *Cancer Lett* **500**, 1–10 (2021).
3. Sun, Y. et al. Abnormal signal pathways and tumor heterogeneity in osteosarcoma. *J. Transl. Med.* **21**(1), 99–110 (2023).
4. Gianferante, D. M. et al. Genetically inferred birthweight, height, and puberty timing and risk of osteosarcoma [J]. *Cancer Epidemiol.* **4**, 124–132 (2023).
5. Cole, S. et al. Osteosarcoma: A surveillance, epidemiology, and end results program-based analysis from 1975 to 2017 [J]. *Cancer* **128**(11), 2107–2118 (2022).
6. Li, S. et al. Targeted therapy for osteosarcoma: A review. *J. Cancer Res. Clin. Oncol.* **149**(9), 6785–6797 (2023).
7. Isakoff, M. S. et al. Osteosarcoma: current treatment and a collaborative pathway to success. *J Clin Oncol: Off J Am Soc Clin Oncol* **33**(27), 3029–3035 (2015).
8. Shoaib, Z., Fan, T. M. & Irudayaraj, J. M. K. Osteosarcoma mechanobiology and therapeutic targets. *Br. J. Pharmacol.* **179**(2), 201–217 (2022).
9. Choi J, Fenando A. Sulfasalazine [M]. StatPearls. Treasure Island (FL) ineligible companies. Disclosure: Ardy Fenando declares no relevant financial relationships with ineligible companies; StatPearls Publishing.
10. Chen, J., Lin, S. & Liu, C. Sulfasalazine for ankylosing spondylitis. *Cochrane Database Syst Rev.* **2014**(11), 21–28 (2014).
11. Mushtaq, S. & Sarkar, R. Sulfasalazine in dermatology: A lesser explored drug with broad therapeutic potential. *Int J Womens Dermatol.* **6**(3), 191–198 (2020).
12. Zhuang, J. et al. Sulfasalazine, a potent suppressor of gastric cancer proliferation and metastasis by inhibition of xCT: Conventional drug in new use. *J. Cell Mol. Med.* **25**(12), 5372–5380 (2021).
13. Sendo, K. et al. Impact of the glutathione synthesis pathway on sulfasalazine-treated endometrial cancer. *Oncotarget* **13**(2), 224–236 (2022).
14. Yin, L. et al. Sulfasalazine inhibits esophageal cancer cell proliferation by mediating ferroptosis. *Chem. Biol. Drug Des.* **102**(4), 730–737 (2023).
15. Takatani-Nakase, T. et al. Regulatory network of ferroptosis and autophagy by targeting oxidative stress defense using sulfasalazine in triple-negative breast cancer. *Life Sci* **339**, 122411 (2024).
16. Zhao, J. et al. Targeting ferroptosis in osteosarcoma. *J Bone Oncol* **30**(3), 100–111 (2021).
17. Zhou, Q. et al. Ferroptosis in cancer: From molecular mechanisms to therapeutic strategies [J]. *Signal Transduct Target Ther* **9**(1), 55–67 (2024).
18. Gao, W. et al. Autophagy, ferroptosis, pyroptosis, and necroptosis in tumor immunotherapy. *Signal Transduct Target Ther* **7**(1), 196–205 (2022).
19. Chen, X. et al. Broadening horizons: The role of ferroptosis in cancer. *Nat Rev Clin Oncol* **18**(5), 280–296 (2021).

20. Lewerenz, J. et al. The cystine/glutamate antiporter system x(c)(-) in health and disease: From molecular mechanisms to novel therapeutic opportunities. *Antioxid. Redox Signal.* **18**(5), 522–555 (2013).
21. Li, D. et al. CST1 inhibits ferroptosis and promotes gastric cancer metastasis by regulating GPX4 protein stability via OTUB1. *Oncogene* **42**(2), 83–98 (2023).
22. Zheng, C. et al. Donafenib and GSK-J4 synergistically induce ferroptosis in liver cancer by upregulating HMOX1 expression. *Adv Sci (Weinh)* **10**(22), e2206798 (2023).
23. Yang, F. et al. Ferroptosis heterogeneity in triple-negative breast cancer reveals an innovative immunotherapy combination strategy. *Cell Metab.* **35**(1), 84–100 (2023).
24. Jiang, M. et al. Exosome-mediated miR-144-3p promotes ferroptosis to inhibit osteosarcoma proliferation, migration, and invasion through regulating ZEB1. *Mol Cancer* **22**(1), 113–121 (2023).
25. Li, Z. et al. Circular RNA circBLNK promotes osteosarcoma progression and inhibits ferroptosis in osteosarcoma cells by sponging miR-188-3p and regulating GPX4 expression. *Oncol. Rep.* **50**(5), 26–38 (2023).
26. Lin, H. et al. EF24 induces ferroptosis in osteosarcoma cells through HMOX1 [J]. *Biomed Pharmacother* **136**(1), 111–120 (2021).
27. Kanehisa, M. et al. KEGG: biological systems database as a model of the real world. *Nucleic Acids Res.* **53**(D1), D672–D677 (2025).
28. Kanehisa, M. Toward understanding the origin and evolution of cellular organisms. *Protein Sci* **28**(11), 1947–1951 (2019).
29. Kanehisa, M. & Goto, S. KEGG: kyoto encyclopedia of genes and genomes. *Nucleic Acids Res.* **28**(1), 27–30 (2000).
30. Gill, J. & Gorlick, R. Advancing therapy for osteosarcoma. *Nat Rev Clin Oncol* **18**(10), 609–624 (2021).
31. Kashyap, D., Garg, V. K. & Goel, N. Intrinsic and extrinsic pathways of apoptosis: Role in cancer development and prognosis. *Adv. Protein Chem. Struct. Biol.* **125**(7), 73–120 (2021).
32. Hänggi, K. & Ruffell, B. Cell death, therapeutics, and the immune response in cancer. *Trends in cancer* **9**(5), 381–396 (2023).
33. Liu, J. et al. Programmed cell death tunes tumor immunity. *Front. Immunol.* **13**(6), 847–852 (2022).
34. Tang, D. et al. Ferroptosis: molecular mechanisms and health implications. *Cell Res.* **31**(2), 107–125 (2021).
35. Liu, J., Kang, R. & Tang, D. Signaling pathways and defense mechanisms of ferroptosis. *FEBS J.* **289**(22), 7038–7050 (2022).
36. Chen, X. et al. Ferroptosis: Machinery and regulation. *Autophagy* **17**(9), 2054–2061 (2021).
37. Koppula, P., Zhuang, L. & Gan, B. Cystine transporter SLC7A11/xCT in cancer: Ferroptosis, nutrient dependency, and cancer therapy. *Protein Cell* **12**(8), 599–620 (2021).
38. Liu, Y. et al. GPX4: The hub of lipid oxidation, ferroptosis, disease and treatment. *Biochim. Biophys. Acta* **1878**(3), 188–198 (2023).
39. Wang, T. et al. Downregulation of lncRNA SLC7A11-AS1 decreased the NRF2/SLC7A11 expression and inhibited the progression of colorectal cancer cells. *PeerJ* **11**(5), e15216–e15227 (2023).
40. Fu, D. et al. Induction of ferroptosis by ATF3 elevation alleviates cisplatin resistance in gastric cancer by restraining Nrf2/Keap1/xCT signaling. *Cell. Mol. Biol. Lett.* **26**(1), 26–38 (2021).
41. Sun, B. et al. A morpholine merivative N-(4-Morpholinomethylene) ethanesulfonamide induces ferroptosis in tumor cells by targeting NRF2. *Biol. Pharm. Bull.* **47**(2), 417–426 (2024).
42. Shi, J. et al. Low-dose antimony exposure promotes prostate cancer proliferation by inhibiting ferroptosis via activation of the Nrf2-SLC7A11-GPX4 pathway. *Chemosphere* **339**(5), 137–142 (2023).
43. Yuan, Y. et al. Kaempferol ameliorates oxygen-glucose deprivation/reoxygenation-induced neuronal ferroptosis by activating Nrf2/SLC7A11/GPX4 Axis [J]. *Biomolecules* **11**(7), 28–39 (2021).
44. Liu, H. et al. Rhein attenuates cerebral ischemia-reperfusion injury via inhibition of ferroptosis through NRF2/SLC7A11/GPX4 pathway. *Exp. Neurol.* **369**(2), 114–121 (2023).
45. Deng, X. et al. Mangiferin attenuates osteoporosis by inhibiting osteoblastic ferroptosis through Keap1/Nrf2/SLC7A11/GPX4 pathway. *Phytomed: Int J Phytother phytopharmacol* **124**(6), 155–163 (2024).

Author contributions

YP and XW designed the study and modified the manuscript. QQ and HB performed the main experiments and wrote the manuscript. ML and JT revised the manuscript. JQ and XC performed some molecular study and analyzed the data. All authors read and approved the final version of the manuscript.

Funding

This study was supported by Gansu province education science and technology innovation project (2022-QB-007), Gansu Provincial Science and Technology Program Joint Research Fund (24JRRG019) and Zhangye Municipal Science and Technology Program Project (ZY2024JS29).

Declarations

Competing interests

The authors declare no conflict of interest.

Additional information

Supplementary Information The online version contains supplementary material available at https://doi.org/10.1038/s41598-025-13324-5.

Correspondence and requests for materials should be addressed to X.W. or Y.W.